Hybrid quantum-state joining and splitting assisted by quantum dots in one-side optical microcavities

Ming-Xing Luo,[1,2,*] Song-Ya Ma,[3,†] Xiu-Bo Chen,[2] and Xiaojun Wang[4]

[1]*Information Security and National Computing Grid Laboratory, School of Information Science and Technology, Southwest Jiaotong University, Chengdu 610031, China*

[2]*State Key Laboratory of Networking and Switching Technology, Beijing University of Posts and Telecommunications, Beijing 100876, China*

[3]*School of Mathematics and Statistics, Henan University, Kaifeng 475004, China*

[4]*School of Electronic Engineering, Dublin City University, Dublin 9, Ireland*

(Received 2 February 2015; published 22 April 2015)

Quantum state joining has been recently experimentally demonstrated [C. Vitelli *et al.*, Nat. Photon. **7**, 521 (2013)] which can transfer two input photonic qubits into a photonic ququart. Here, we revisit these processes from a hybrid point of view. By exploring the giant optical circular birefringence induced by quantum-dot spins in one-sided optical microcavities, we introduce some deterministic joining schemes including two quantum-dot spin joining, hybrid photon and quantum-dot spin joining, and two-photon joining. The input quantum information is represented by one photon with polarization and spatial mode degrees of freedom (DOFs). These schemes are also adapted to the inverse processes called quantum state splitting because all the joining procedures are unitary and do not require projection and feed-forward steps. The fused photon is convenient for realizing elementary logic gates such as the controlled-NOT (CNOT) gate, SWAP gate, and Toffoli gate. These hybrid fusion and splitting schemes provide flexible synthesis of the quantum-dot spin and photon in quantum applications. The transmission superiority of photons and storage superiority of the quantum-dot spin may be combined for quantum network communication or quantum computations.

DOI: 10.1103/PhysRevA.91.042326 PACS number(s): 03.67.Hk, 03.65.Ud, 42.50.Pq

I. INTRODUCTION

Quantum information, based on quantum mechanics theory, provides an opportunity to enhance computational power [1–4] and build the secure communication [5–10]. To physically realize these applications, multiple qubits should be processed simultaneously. However, the photonic approaches based on qubit states [11–14] are in practice limited to small qubits by the present experimental technology [15–18]. The multiple DOFs of one photon may be an alternative approach to reduce the processing difficulty caused by the large number of photons. By making use of polarization, time bin, wavelength, or transverse modes of one photon, quantum information may be represented in enlarged state spaces [19–24] with independent multiple DOFs [25,26]. This approach may substantially increase the number of qubits [27,28]. These two methods may be combined flexibly depending on specific requirements in various quantum applications.

Recently, C. Vitelli *et al.* [29] probabilistically combined two photonic qubits into a single photon within a four-dimensional quantum space using linear quantum optics [30–32]. They called this quantum process "quantum state joining" or fusion. The inverse process, i.e., quantum splitting, was also proposed. Both processes have been theoretically reinvestigated and improved to deterministic schemes [33]. Because of their iterability, those schemes may convert a multi-photon encoding of quantum information into a single-photon higher-dimensional one and vice versa. Moreover, photonic qubit joining has to require at least one ancillary photon using linear quantum optics. These fusion processes may be applied to multiplex and demultiplex the quantum information in photons [34,35], a matter-based quantum register [36,37], and quantum-information networks [38,39].

In particular, quantum state joining and splitting rely on the existence of hypothetical controlled-NOT (CNOT) gates in encoding photons [30,33]. The CNOT gate as a primitive gate to construct universal quantum circuits has been intensively implemented using a linear optics system [30–32], Josephson charge qubits in superconducting circuit [40,41], and nuclear magnetic resonance [42,43]. Recently, the solid-state quantum system based on a quantum-dot spin in a quantum dot (QD) inside a microcavity has attracted much attention because of its optical property and scalability. The quantum interaction between photons and spins in QDs can be promoted by the structure of a cavity-QD system. In a weak-coupling cavity, the electron-spin-cavity system works like a beam splitter in the limit of a weak incoming field [44,45]. The spin photon interface has been widely used to generate universal gates [26,27,46–48], hybrid entanglement [49–51], and Bell-state analyzers [26,51–53]. The fidelity and efficiency have also been investigated in weak and strong coupling regimes. These schemes could be realized with current physical technology [54–61].

In this paper, we consider the quantum state joining of the quantum-dot spin and photon. In comparison to the probabilistic joining experiment of two photons with linear optics [29], we propose the deterministic fusion of two quantum spins, the deterministic fusion of one photon and one quantum-dot spin, and the deterministic fusion of two photons with the help of quantum dots embedded in a microcavity. The quantum-dot spin may be a charged self-assembled GaAs/InAs quantum dot in a micropillar resonator [45–61]. The first scheme may be

*mxluo@home.swjtu.edu.cn
†masongya0829@126.com

viewed as an experimental joining of quantum-dot spins. The second one is a hybrid implementation of quantum joining. The last is a deterministic photonic scheme with the help of cavity-QD systems. All target ququarts are represented by one photon with two DOFs, i.e., the circular polarization DOF and spatial-mode DOF. Furthermore, all the joining schemes may be modified into unitary schemes, which are applicable in quantum state splitting cases. Our joining and splitting schemes may provide candidates for quantum communication and quantum computation because they allow exploiting different quantum systems at the best of their potentials.

The paper is organized as follows. In Sec. II, we introduce the photon-matter platform based on a singly charged QD located in the center of a one-sided optical resonant cavity. In Sec. III, the quantum spin joining schemes are realized by adopting quantum-dot spins in one-sided optical microcavities. It may be completed with the projection and feed-forward mechanism or no-postselection mechanism (more quantum correlation operations). In Sec. IV, the quantum joining scheme is realized with one quantum-dot spin and one photon using auxiliary one-sided optical microcavities in both the postselection and no-postselection mechanisms. And then, the photonic joining scheme is realized in Sec. V in both postselection and no-postselection mechanisms. All present joining schemes are modified to quantum splitting schemes by choosing the no-postselection mechanisms. In Sec. VI, the fused photon is used to realize elementary gates such as the CNOT gate, SWAP gate, and Toffoli gate. In Sec. VII, we analyze experimental feasibilities and fidelities of these schemes with the current technology.

II. QUANTUM-DOT-CAVITY SYSTEM

The QD-cavity system used in this paper is constructed by a singly charged QD such as a self-assembled In(Ga)As QD or a GaAs interface QD [49,50,57], which is located in a one-sided optical resonant cavity. The bottom distributed Bragg reflectors are completely reflective while the top distributed Bragg reflectors are partially reflective. Due to Pauli's exclusion principle, a negatively charged exciton X^- consisting of two electrons [45,53,57,62] can be optically excited when an excess electron is injected into the QD. The optical resonance of X^- with circularly polarized photons depends on the excess electron spin in the QD, shown in Fig. 1. For the excess electron-spin state $|\uparrow\rangle$ with $J_z = +\frac{1}{2}$, the negatively charged exciton $|\uparrow\downarrow\Uparrow\rangle$ is created by resonantly absorbing a left circularly polarized photon $|L\rangle$. For the excess electron spin $|\downarrow\rangle$ with $J_z = -\frac{1}{2}$, the other negatively charged exciton $|\downarrow\uparrow\Downarrow\rangle$ can be created by resonantly absorbing a right circularly polarized photon $|R\rangle$. Here, $|\Uparrow\rangle$ and $|\Downarrow\rangle$ describe heavy-hole spin states with $J_z = +\frac{3}{2}$ and $J_z = -\frac{3}{2}$, respectively.

The input-output relation of this QD-cavity system can be calculated from the Heisenberg equations [62] for the cavity field operator $\hat{a}$ and dipole operator σ_-,

$$\begin{aligned}\frac{d}{dt}\hat{a} &= -\left(i\Delta\omega_c + \frac{\eta}{2} + \frac{\eta_s}{2}\right)\hat{a} - g\hat{\sigma}_- - \sqrt{\eta}\hat{a},\\ \frac{d}{dt}\hat{\sigma}_- &= -\left(i\Delta\omega_x + \frac{\varsigma}{2}\right)\hat{\sigma}_- - g\hat{\sigma}_z\hat{a},\\ \hat{a}_{\rm out} &= \hat{a}_{\rm in} + \sqrt{\eta}\hat{a},\end{aligned} \tag{1}$$

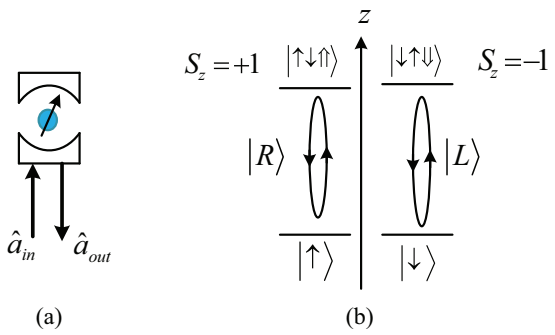

FIG. 1. (Color online) (a) A charged QD inside an one-sided micropillar microcavity interacting with circularly polarized photons. $\hat{a}_{\rm in}$ and $\hat{a}_{\rm out}$ are the input and output field operators of the waveguide, respectively. (b) Optical selection rules due to the Pauli exclusion principle.

where $\Delta\omega_c = \omega_c - \omega$ and $\Delta\omega_x = \omega_{X^-} - \omega$. ω_c, ω, and ω_{X^-} are the frequencies of the cavity mode, input probe light, and X^- transition, respectively. g is the coupling strength between the cavity and X^-. $\varsigma/2$, $\eta/2$, and $\eta_s/2$ are the decay rates of the X^-, cavity field, and cavity side leakage mode, respectively. $\hat{a}_{\rm in}$ and $\hat{a}_{\rm out}$ are the input and output field operators, respectively. If X^- stays in the ground state most of the time [45,53,57,62] [$\langle\sigma_Z\rangle = -1$], the cavity output $\hat{a}_{\rm out}$ is connected with the input by the standard input-output relation

$$\hat{a}_{\rm out} \approx r(\omega)\hat{a}_{\rm in}, \tag{2}$$

where $r(\omega) = 1 - \frac{2\eta}{i2\Delta\omega_c + \eta_s + \eta + 2\hat{g}}$ is the reflection coefficient of the cavity system. $\hat{g} = g^2/(i\Delta\omega_x + \varsigma/2)$. Considering the coupling strength $g = 0$, the QD is uncoupled from the cavity (the cold cavity), thus the reflection coefficient of the QD-cavity system is defined as

$$r_0(\omega) = 1 - \frac{2\eta}{i2\Delta\omega_c + \eta_s + \eta}. \tag{3}$$

In the strong coupling regime $g \gg (\eta, \varsigma)$, the X^- state and cavity mode are mixed to form two new states, i.e., the dressed states, which leads to the vacuum-Rabi splitting. The strongly coupled cavity system is called a hot cavity. We work near the resonant condition with $|\Delta\omega_c| \ll g$ so that $|r(\omega)| \approx 1$ holds for both the cold and the hot cavity. If the excess electron lies in the spin state $|\uparrow\rangle$, the light $|L\rangle$ feels the hot cavity and gets a phase shift of $\theta_f = \arg[r(\omega)]$ after reflection, whereas the light $|R\rangle$ feels the cold cavity and gets a phase shift of $\theta_0 = \arg[r_0(\omega)]$. Conversely, if the excess electron lies in the spin state $|\downarrow\rangle$, the light $|R\rangle$ feels the hot cavity and gets a phase shift of θ_f after reflection, whereas the light $|L\rangle$ feels the cold cavity and gets a phase shift of θ_0. Thus, two phase shifts may be gotten as

$$\begin{aligned}&|R\rangle|\uparrow\rangle \to e^{i\theta_0}|R\rangle|\uparrow\rangle, \quad |R\rangle|\downarrow\rangle \to e^{i\theta_f}|R\rangle|\downarrow\rangle,\\ &|L\rangle|\uparrow\rangle \to e^{i\theta_f}|L\rangle|\uparrow\rangle, \quad |L\rangle|\downarrow\rangle \to e^{i\theta_0}|L\rangle|\downarrow\rangle.\end{aligned} \tag{4}$$

When the side leakage and cavity loss are ignored ($\eta_s = 0$), by adjusting the frequencies $\Delta\omega_c/\eta \to 0$ and $\Delta\omega_x/\eta \to 0$ we can get the phase shifts $\theta_0 = \pi$ and $\theta_f = 0$ for $g^2 \gg \eta\varsigma$. Thus the dynamics of the interaction between photon and electron in

a microcavity coupled system [63,64] are described as follows:

$$|R\rangle|\uparrow\rangle \to -|R\rangle|\uparrow\rangle, \quad |R\rangle|\downarrow\rangle \to |R\rangle|\downarrow\rangle,$$
$$|L\rangle|\uparrow\rangle \to |L\rangle|\uparrow\rangle, \quad |L\rangle|\downarrow\rangle \to -|L\rangle|\downarrow\rangle. \tag{5}$$

In the following, this spin-cavity unit is used to join quantum-dot spin and photon for efficient quantum-information processing.

III. QUANTUM-DOT SPIN JOINING

C. Vitelli *et al.* [29] proposed probabilistic photon joining scheme using linear quantum optics. For two input photon states

$$|\phi_1\rangle = \alpha|H\rangle + \beta|V\rangle, \quad |\phi_2\rangle = \gamma|H\rangle + \delta|V\rangle, \tag{6}$$

where $|H\rangle$ and $|V\rangle$ denote the states of horizontal and vertical linear polarization, corresponding to the logical 0 and 1, respectively. The joint system may be rewritten as

$$\begin{aligned}|\phi_1\rangle|\phi_2\rangle &= \alpha\gamma|HH\rangle + \alpha\delta|HV\rangle + \beta\gamma|VH\rangle + \beta\delta|VV\rangle \\ &:= \alpha\gamma|0\rangle + \alpha\delta|1\rangle + \beta\gamma|2\rangle + \beta\delta|3\rangle\end{aligned} \tag{7}$$

by using quantum state joining, which transforms a two-photon system into a single-photon one. Here, $\{|0\rangle,|1\rangle,|2\rangle,|3\rangle\}$ is an arbitrary orthogonal basis in a four-dimensional space. They combined two photons into a photon of the polarization DOF and spatial mode DOF with the success probability 1/8. By using some additional CNOT gates, the success probability has been improved to 1 in theory [33]. They introduced some modified theoretical schemes without projection and feed-forward steps. This is very important in the quantum state splitting case. Moreover, they formally proved that the quantum joining of two photon states with linear optics requires the use of at least one ancillary photon.

In this section, we consider two quantum-dot spins $|\psi_1\rangle_{e_i}$ located in the one-sided cavity$_i$ (denoted as Cy$_i$) as the input qubits, where

$$|\psi_1\rangle_{e_1} = \alpha|\uparrow\rangle + \beta|\downarrow\rangle, \quad |\psi_2\rangle_{e_2} = \gamma|\uparrow\rangle + \delta|\downarrow\rangle. \tag{8}$$

Using the one-sided cavity, we can perfectly join two spins into a photon with the circular polarization DOF and spatial mode DOF. The detailed fusion circuit of $|\psi_1\rangle|\psi_2\rangle$ is shown in Fig. 2(a). An auxiliary photon A in the state $|R\rangle|a_1\rangle$ passes from the half-wave plate H_1 to the 50:50 beam splitters cBS$_2$, sequentially. The joint system of two spins e_i and the photon A is changed as

$$\begin{aligned}|R\rangle_A|a_1\rangle|\psi_1\rangle_{e_1}|\psi_2\rangle_{e_2} &\xrightarrow{H_1} \frac{1}{\sqrt{2}}(|R\rangle + |L\rangle)_A|a_1\rangle|\psi_1\rangle_{e_1}|\psi_2\rangle_{e_2} \\ &\xrightarrow[\text{cPS}_2]{\text{cPS}_1,\text{Cy}_1} \frac{1}{\sqrt{2}}[\alpha(|R\rangle + |L\rangle)_A|\uparrow\rangle_{e_1} + \beta(|R\rangle - |L\rangle)_A|\downarrow\rangle_{e_1}]|a_1\rangle|\psi_2\rangle_{e_2} \\ &\xrightarrow{H_2} (\alpha|R\rangle_A|\uparrow\rangle_{e_1} + \beta|L\rangle_A|\downarrow\rangle_{e_1})|a_1\rangle|\psi_2\rangle_{e_2} \\ &\xrightarrow{\text{cBS}_1} (\alpha|R\rangle_A|\uparrow\rangle_{e_1} + \beta|L\rangle_A|\downarrow\rangle_{e_1}) \otimes \frac{1}{\sqrt{2}}(|a_1\rangle + |a_2\rangle)|\phi_2\rangle_{e_2} \\ &\xrightarrow[\text{cPS}_4]{\text{cPS}_3,\ldots,} (\alpha|R\rangle_A|\uparrow\rangle_{e_1} + \beta|L\rangle_A|\downarrow\rangle_{e_1}) \otimes \frac{1}{\sqrt{2}}[\gamma(|a_1\rangle + |a_2\rangle)|\uparrow\rangle_{e_2} + \delta(|a_1\rangle - |a_2\rangle)|\downarrow\rangle_{e_2}] \\ &\xrightarrow{\text{cBS}_2} (\alpha|R\rangle_A|\uparrow\rangle_{e_1} + \beta|L\rangle_A|\downarrow\rangle_{e_1}) \otimes (\gamma|a_1\rangle|\uparrow\rangle_{e_2} + \delta|a_2\rangle|\downarrow\rangle_{e_2}),\end{aligned} \tag{9}$$

which may collapse into one photon state with two DOFs as follows:

$$(\alpha|R\rangle + \beta|L\rangle)_A \otimes (\gamma|a_1\rangle + \delta|a_2\rangle) := \alpha\gamma|R_1\rangle + \beta\gamma|L_1\rangle + \alpha\delta|R_2\rangle + \beta\delta|L_2\rangle, \tag{10}$$

using two quantum-dot spin measurements M_{e_1} and M_{e_2} under the basis $\{|\pm\rangle\}$ and some feedback transformations. Here, $|R_i\rangle := |R\rangle|a_i\rangle$ and $|L_i\rangle := |L\rangle|a_i\rangle$. The phase flip (Pauli Z) should be performed on the polarization DOF of the photon A for the measurement outcome $|-\rangle$ of the spin e_1 or on the spatial mode DOF of the photon A for the measurement outcome $|-\rangle$ of the spin e_2. Thus the quantum-dot spin joining has deterministically completed in the ideal conditions.

The quantum-dot spins e_i and the photon A are entangled under the spin-cavity interactions. They may be disentangled with the quantum-dot spin measurements M_{e_1} and M_{e_2} and feedback transformations above. This fusion procedure is not invertible. Fortunately, M_{e_1} and M_{e_2} may be avoided using additional spin-cavity interactions. The detailed disentangling circuit is shown in Fig. 2(b). The joint system shown in the Eq. (9) is the initial system for the disentangling procedure. The detailed evolution procedure is defined as follows.

$$\begin{aligned}&(\alpha|R\rangle_A|\uparrow\rangle_{e_1} + \beta|L\rangle_A|\downarrow\rangle_{e_1})(\gamma|a_1\rangle|\uparrow\rangle_{e_2} + \delta|a_2\rangle|\downarrow\rangle_{e_2}) \\ &\xrightarrow{W_1} \frac{1}{\sqrt{2}}[(\alpha|R\rangle_A + \beta|L\rangle_A)|\uparrow\rangle_{e_1} + (\alpha|R\rangle_A - \beta|L\rangle_A)|\downarrow\rangle_{e_1}] \otimes (\gamma|a_1\rangle|\uparrow\rangle_{e_2} + \delta|a_2\rangle|\downarrow\rangle_{e_2})\end{aligned}$$

$$\xrightarrow[\text{cPS}_6]{\text{cPS}_5,\text{Cy}_1} \frac{1}{\sqrt{2}}\gamma(\alpha|R\rangle_A+\beta|L\rangle_A)|a_1\rangle|\uparrow\rangle_{e_1}|\uparrow\rangle_{e_2}+\frac{1}{\sqrt{2}}\gamma(\alpha|R\rangle_A+\beta|L\rangle_A)|a_1\rangle|\downarrow\rangle_{e_1}|\uparrow\rangle_{e_2}$$
$$+\frac{1}{\sqrt{2}}\delta(\alpha|R\rangle_A+\beta|L\rangle_A)|a_2\rangle|\uparrow\rangle_{e_1}|\downarrow\rangle_{e_2}+\frac{1}{\sqrt{2}}\delta(\alpha|R\rangle_A-\beta|L\rangle_A)|a_2\rangle|\downarrow\rangle_{e_1}|\downarrow\rangle_{e_2}$$
$$\xrightarrow[\text{cPS}_8]{\text{cPS}_7,\text{Cy}_1}(\alpha|R\rangle_A+\beta|L\rangle_A)|+\rangle_{e_1}\otimes(\gamma|a_1\rangle|\uparrow\rangle_{e_2}+\delta|a_2\rangle|\downarrow\rangle_{e_2})$$
$$\xrightarrow{W_2}(\alpha|R\rangle_A+\beta|L\rangle_A)|\uparrow\rangle_{e_1}\otimes(\gamma|a_1\rangle|\uparrow\rangle_{e_2}+\delta|a_2\rangle|\downarrow\rangle_{e_2})$$
$$\xrightarrow{W_3}\frac{1}{\sqrt{2}}(\alpha|R\rangle_A+\beta|L\rangle_A)|\uparrow\rangle_{e_1}\otimes[(\gamma|a_1\rangle+\delta|a_2\rangle)|\uparrow\rangle_{e_2}+(\gamma|a_1\rangle-\delta|a_2\rangle)|\downarrow\rangle_{e_2}]$$
$$\xrightarrow[X_4,\text{cPS}_{10}]{\text{cPS}_9,X_3,\text{Cy}_2}(\alpha|R\rangle_A+\beta|L\rangle_A)(\gamma|a_1\rangle+\delta|a_2\rangle)|\uparrow\rangle_{e_1}|+\rangle_{e_2}$$
$$\xrightarrow{W_4}(\alpha|R\rangle_A+\beta|L\rangle_A)(\gamma|a_1\rangle+\delta|a_2\rangle)|\uparrow\rangle_{e_1}|\uparrow\rangle_{e_2}. \tag{11}$$

Therefore, by combining the circuits shown in Figs. 2(a) and 2(b), two quantum-dot spins can be joined into one photon state with two DOFs without any measurement feedback. Thus the quantum fusion scheme is unitary.

IV. HYBRID JOINING THE PHOTON AND QUANTUM-DOT SPIN

In comparison to the photonic state fusion [29] and the quantum-dot spin fusion in Sec. III, the photon and quantum-dot spin may be joined into a photon state assisted by a one-sided cavity. The initial photon B and the quantum-dot spin e (located in the cavity Cy) are defined as

$$|\phi\rangle_B=\alpha|R\rangle+\beta|L\rangle,\quad |\psi\rangle_e=\gamma|\uparrow\rangle+\delta|\downarrow\rangle, \tag{12}$$

respectively. The hybrid fusion circuit of $|\phi\rangle_B|\psi\rangle_e$ is shown in Fig. 3(a), using an auxiliary photon A in the state $|R\rangle_A|a_1\rangle$ and an auxiliary quantum-dot spin e' in the state $|+\rangle_{e'}$. Two photons A and B pass from the cPS_1 to cBS_2 sequentially. The joint system of the photons A and B and two spins e and e' changes as follows.

$$|\phi\rangle_B|\psi\rangle_e|R\rangle_A|a_1\rangle|+\rangle_{e'}\xrightarrow[\text{cPS}_2]{\text{cPS}_1,\text{Cy}_1}\frac{1}{\sqrt{2}}[(\alpha|R\rangle+\beta|L\rangle)_B|\uparrow\rangle_{e'}+(\alpha|R\rangle-\beta|L\rangle)_B|\downarrow\rangle_{e'}]|R\rangle_A|a_1\rangle|\psi\rangle_e$$
$$\xrightarrow{W_1}(\alpha|R\rangle_B|\uparrow\rangle_{e'}+\beta|L\rangle_B|\downarrow\rangle_{e'})|R\rangle_A|a_1\rangle|\psi\rangle_e$$
$$\xrightarrow{H_1}\frac{1}{\sqrt{2}}(\alpha|R\rangle_B|\uparrow\rangle_{e'}+\beta|L\rangle_B|\downarrow\rangle_{e'})\otimes(|R\rangle+|L\rangle)_A|a_1\rangle|\psi\rangle_e$$
$$\xrightarrow[\text{cPS}_4]{\text{cPS}_3,\text{Cy}_1}\frac{1}{\sqrt{2}}[\alpha|R\rangle_B|\uparrow\rangle_{e'}(|R\rangle+|L\rangle)_A+\beta|L\rangle_B|\downarrow\rangle_{e'}(|R\rangle-|L\rangle)_A]|a_1\rangle|\psi\rangle_e$$
$$\xrightarrow{H_2}(\alpha|R\rangle_B|\uparrow\rangle_{e'}|R\rangle_A+\beta|L\rangle_B|\downarrow\rangle_{e'}|L\rangle_A)|a_1\rangle|\psi\rangle_e$$
$$\xrightarrow{\text{cBS}_1}(\alpha|R\rangle_B|\uparrow\rangle_{e'}|R\rangle_A+\beta|L\rangle_B|\downarrow\rangle_{e'}|L\rangle_A)\otimes\frac{1}{\sqrt{2}}(|a_1\rangle+|a_2\rangle)|\psi\rangle_e$$
$$\xrightarrow[\text{cPS}_6]{\text{cPS}_5,\ldots,}(\alpha|R\rangle_B|\uparrow\rangle_{e'}|R\rangle_A+\beta|L\rangle_B|\downarrow\rangle_{e'}|L\rangle_A)\otimes\frac{1}{\sqrt{2}}[\gamma(|a_1\rangle+|a_2\rangle)|\uparrow\rangle_e+\delta(|a_1\rangle-|a_2\rangle)|\downarrow\rangle_e]$$
$$\xrightarrow{\text{cBS}_2}(\alpha|R\rangle_B|\uparrow\rangle_{e'}|R\rangle_A+\beta|L\rangle_B|\downarrow\rangle_{e'}|L\rangle_A)\otimes(\gamma|a_1\rangle|\uparrow\rangle_e+\delta|a_2\rangle|\downarrow\rangle_e), \tag{13}$$

which may collapse into one photon state with two DOFs as follows:

$$(\alpha|R\rangle_A+\beta|L\rangle_A)(\gamma|a_1\rangle+\delta|a_2\rangle)$$
$$:=\alpha\gamma|R_1\rangle+\beta\gamma|L_1\rangle+\alpha\delta|R_2\rangle+\beta\delta|L_2\rangle \tag{14}$$

using the measurements $M_{e'}$, M_e, and M_B, and some feedback transformations. Here, $M_{e'}$ and M_e are the spin measurements under the basis $\{|\pm\rangle\}$, and M_B denotes the single photon measurement under the basis $\{\frac{1}{\sqrt{2}}(|R\rangle\pm|L\rangle)\}$. For the measurement outcome $|-\rangle$ of the spin e' and $\frac{1}{\sqrt{2}}(|R\rangle-|L\rangle)$ of photon B, the phase flip (Pauli Z) should be performed on the polarization DOF of the photon A. For the measurement outcome $|-\rangle$ of spin e, the Pauli Z should be performed on the spatial mode DOF of photon A. The subcircuit (photon A passing through the cBS_1, X_1, Cy, X_2, and cBS_2, sequentially) of photon A and the quantum-dot spin e is similar to the

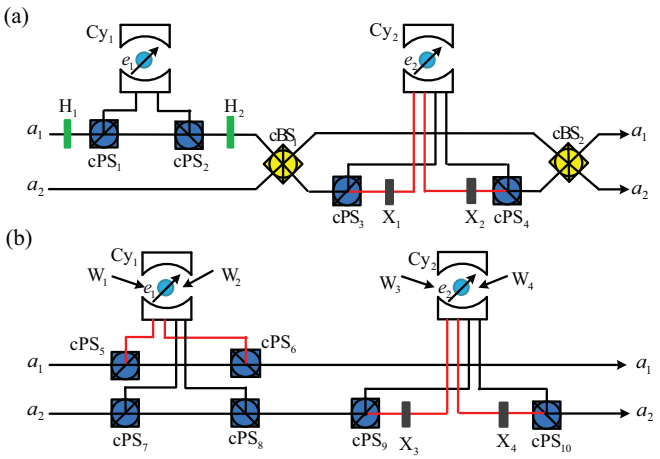

FIG. 2. (Color online) (a) Quantum spin fusion in a postselection mechanism. cPS_i represent the circularly polarizing beam splitters that transmit the right circularly polarizing photon $|R\rangle$ and reflect the left circularly polarizing $|L\rangle$, respectively. a_i denote the spatial modes of the auxiliary photon A. e_i denote quantum-dot spins with initial states $|\psi_i\rangle$. H_i denote the half-wave plates to perform the Hadamard transformation $|R\rangle \rightarrow \frac{1}{\sqrt{2}}(|R\rangle + |L\rangle)$ and $|L\rangle \rightarrow \frac{1}{\sqrt{2}}(|R\rangle - |L\rangle)$. X_i denote the wave plates to perform the polarization flip transformation $|R\rangle\langle L| + |L\rangle\langle R|$. cBS_i represent the 50:50 beam splitters to perform the Hadamard operation $|a_1\rangle \rightarrow \frac{1}{\sqrt{2}}(|a_1\rangle + |a_2\rangle)$ and $|a_2\rangle \rightarrow \frac{1}{\sqrt{2}}(|a_1\rangle - |a_2\rangle)$ on the spatial mode DOF of the photon. (b) Quantum spin disentangling. W_i denote the Hadamard transformation $|\uparrow\rangle \rightarrow |+\rangle = \frac{1}{\sqrt{2}}(|\uparrow\rangle + |\downarrow\rangle)$ and $|\downarrow\rangle \rightarrow |-\rangle = \frac{1}{\sqrt{2}}(|\uparrow\rangle - |\downarrow\rangle)$ performed on the spins. If there are two input lines of one cavity, the photon represented with red lines passes through the cavity first, and then the photon represented with black lines passes through the cavity.

subcircuit (photon A passing through the cBS_1, cPS_3, X_1, Cy_2, X_2, cPS_4, and cBS_2, sequentially) of photon A and the quantum-dot spin e_2 defined in Fig. 2(a), which has realized the CNOT gate on the spin and the spatial mode DOF of the photon, i.e.,

$$|\uparrow\rangle\langle\uparrow|(|a_1\rangle\langle a_1| + |a_2\rangle\langle a_2|) + |\downarrow\rangle\langle\downarrow|(|a_2\rangle\langle a_1| + |a_1\rangle\langle a_2|). \tag{15}$$

Thus the hybrid photon and spin fusion has completed.

Similar to the disentangling circuit shown in Fig. 2(b), the spin measurements M_e and $M_{e'}$ and the photon measurement M_B may be avoided in order to get invertible fusion procedure. The detailed disentangling circuit is shown in Fig. 3(b). The evolution procedure for the entanglement shown in Eq. (13) is defined as follows.

$$\begin{aligned}
&(\alpha|R\rangle_B|\uparrow\rangle_{e'}|R\rangle_A + \beta|L\rangle_B|\downarrow\rangle_{e'}|L\rangle_A)(\gamma|a_1\rangle|\uparrow\rangle_e + \delta|a_2\rangle|\downarrow\rangle_e)\\
&\xrightarrow{H_3,\ldots,H_4} |R\rangle_B(\alpha|\uparrow\rangle_{e'}|R\rangle_A + \beta|\downarrow\rangle_{e'}|L\rangle_A)\\
&\qquad\otimes(\gamma|\uparrow\rangle_e|a_1\rangle + \delta|\downarrow\rangle_e|a_2\rangle)\\
&\xrightarrow{W_2,\ldots,W_3} |R\rangle_B|\uparrow\rangle_{e'}(\alpha|R\rangle_A + \beta|L\rangle_A)\\
&\qquad\otimes(\gamma|\uparrow\rangle_e|a_1\rangle + \delta|\downarrow\rangle_e|a_2\rangle)\\
&\xrightarrow{W_4,\ldots,W_5} (\alpha|R\rangle_A + \beta|L\rangle_A)(\gamma|a_1\rangle + \delta|a_2\rangle)\\
&\qquad\otimes|R\rangle_B|\uparrow\rangle_{e'}|\uparrow\rangle_e.
\end{aligned} \tag{16}$$

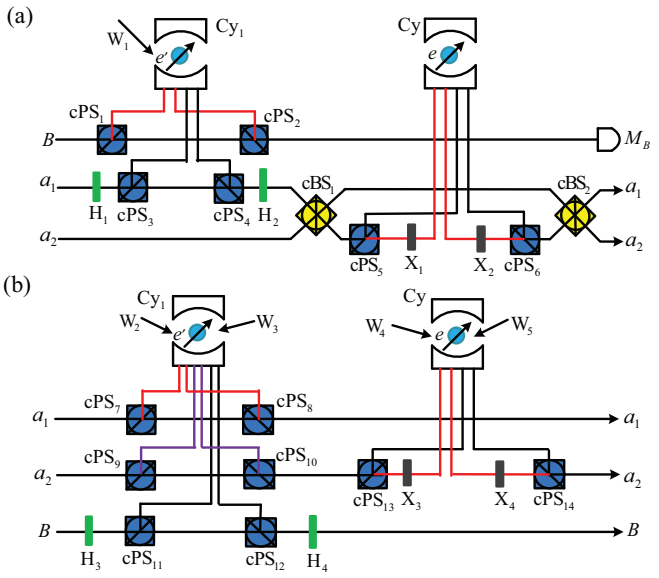

FIG. 3. (Color online) (a) Hybrid joining scheme based on the measurement feedback. e' denotes an auxiliary quantum-dot spin in the state $|+\rangle$ located in the cavity Cy_1. cPS_i, H_i, X_i, cBS_i, and W_i are the same as those defined in Fig. 2. (b) Schematic disentangling. If there are two input lines of one cavity, the photon represented with red lines passes through the cavity first, and then the photon represented with black lines passes through the cavity. If there are three input lines of one cavity, the photon represented with red lines passes through the cavity first, and then the photon represented with purple lines passes through the cavity while the photon represented with black lines passes through the cavity last.

Here, the subcircuit (photon B passing through the H_3, cPS_3, Cy_1, cPS_4, and H_4, sequentially) of the photon B and the quantum-dot spin e' is the same as the subcircuit (photon A passing through the H_1, cPS_1, Cy_1, cPS_2, and H_2, sequentially) of photon A and the quantum-dot spin e_1 shown in Fig. 2(a), which has realized the CNOT gate

$$|\uparrow\rangle\langle\uparrow|(|R\rangle\langle R| + |L\rangle\langle L|) + |\downarrow\rangle\langle\downarrow|(|R\rangle\langle L| + |L\rangle\langle R|) \tag{17}$$

operated on the spin and polarization DOF of the photon. The subcircuit (photon A passing through the W_2, cPS_7, Cy_1, cPS_8, cPS_9, Cy_1, cPS_{10}, and W_3, sequentially) of photon A and the quantum-dot spin e' is the same as the subcircuit (the photon A passing through the W_1, cPS_5, Cy_1, cPS_6, cPS_7, Cy_1, cPS_8, and W_2, sequentially) of photon A and the quantum-dot spin e_1 shown in Fig. 2(b), which has realized the CNOT gate

$$|R\rangle\langle R|(|\uparrow\rangle\langle\uparrow| + |\downarrow\rangle\langle\downarrow|) + |L\rangle\langle L|(|\uparrow\rangle\langle\downarrow| + |\downarrow\rangle\langle\uparrow|) \tag{18}$$

operated on the polarization DOF of the photon and the spin. The subcircuit (photon A passing through the W_4, cPS_{13}, X_3, Cy, X_4, cPS_{14}, and W_5, sequentially) of photon A and the quantum-dot spin e is the same as the subcircuit (photon A passing through the W_3, cPS_9, X_3, Cy_2, X_4, cPS_{10}, and W_4, sequentially) of photon A and the quantum-dot spin e_2 shown in Fig. 2(b), which has realized the CNOT gate

$$|a_1\rangle\langle a_1|(|\uparrow\rangle\langle\uparrow| + |\downarrow\rangle\langle\downarrow|) + |a_2\rangle\langle a_2|(|\uparrow\rangle\langle\downarrow| + |\downarrow\rangle\langle\uparrow|) \tag{19}$$

operated on the spatial mode DOF of the photon and the spin. Therefore, by combining the circuits shown in Fig. 3, one

photon and one spin can be joined into one photon state with two DOFs without postselection. The hybrid fusion is unitary.

V. PHOTON FUSION

In comparison to probabilistic photon fusion [29] with linear optics, deterministic photon joining may be completed with the help of the one-sided cavity. The input photons are defined as

$$|\phi_1\rangle_B = \alpha|R\rangle + \beta|L\rangle, \quad |\phi_2\rangle_C = \gamma|R\rangle + \delta|L\rangle. \tag{20}$$

The detailed fusion circuit of $|\phi_1\rangle|\phi_2\rangle$ is shown in Fig. 4(a), using two auxiliary quantum-dot spins e_i in the state $|+\rangle$. From Eqs. (13), (15), and (17), the joint system of photons A and B and auxiliary spins e_1 and e_2 changes as follows:

$$\begin{aligned}
&|\phi_1\rangle_B|\phi_2\rangle_C|R\rangle_A|a_1\rangle|+\rangle_{e_1}|+\rangle_{e_2}\\
&\xrightarrow[\mathrm{cPS}_2,W_1]{\mathrm{cPS}_1,\mathrm{Cy}_1} (\alpha|R\rangle_B|\uparrow\rangle_{e_1} + \beta|L\rangle_B|\downarrow\rangle_{e_1})|R\rangle_A|a_1\rangle\\
&\quad \otimes|\phi_2\rangle_C|+\rangle_{e_2}\\
&\xrightarrow[\mathrm{cPS}_4,H_2]{H_1,\mathrm{cPS}_3,\mathrm{Cy}_1} (\alpha|R\rangle_A|R\rangle_B|\uparrow\rangle_{e_1} + \beta|L\rangle_A|L\rangle_B|\downarrow\rangle_{e_1})|a_1\rangle\\
&\quad \otimes|\phi_2\rangle_C|+\rangle_{e_2}\\
&\xrightarrow[X_2,\mathrm{cBS}_2]{\mathrm{cBS}_1,X_1,\mathrm{Cy}_1} (\alpha|R\rangle_A|R\rangle_B|\uparrow\rangle_{e_1} + \beta|L\rangle_A|L\rangle_B|\downarrow\rangle_{e_1})\\
&\quad \otimes(|a_1\rangle|\uparrow\rangle_{e_2} + |a_2\rangle|\downarrow\rangle_{e_2})|\phi_2\rangle_C\\
&\xrightarrow[\mathrm{cPS}_8,W_2]{\mathrm{cPS}_7,\mathrm{Cy}_2} (\alpha|R\rangle_A|R\rangle_B|\uparrow\rangle_{e_1} + \beta|L\rangle_A|L\rangle_B|\downarrow\rangle_{e_1})\\
&\quad \otimes(\gamma|R\rangle_C|a_1\rangle|\uparrow\rangle_{e_2} + \delta|L\rangle_C|a_2\rangle|\downarrow\rangle_{e_2}).
\end{aligned} \tag{21}$$

This state may collapse into

$$\begin{aligned}
&(\alpha|R\rangle_A + \beta|L\rangle_A)(\gamma|a_1\rangle + \delta|a_2\rangle)\\
&:= \alpha\gamma|R_1\rangle + \beta\gamma|L_1\rangle + \alpha\delta|R_2\rangle + \beta\delta|L_2\rangle,
\end{aligned} \tag{22}$$

using the measurement M_{e_i}, M_B, and M_C, and feed-forward transformations. Here, M_{e_i} denotes the measurement of the spin e_i under the basis $\{|\pm\rangle\}$, M_B and M_C denote the measurements of photons B and C under the basis $\{\frac{1}{\sqrt{2}}(|R\rangle \pm |L\rangle)\}$, respectively. For the measurement outcome $|-\rangle_{e_1}$ or $\frac{1}{\sqrt{2}}(|R\rangle - |L\rangle)_B$, the phase flip should be performed on the polarization DOF of photon A. For the measurement outcome $|-\rangle_{e_2}$ or $\frac{1}{\sqrt{2}}(|R\rangle - |L\rangle)_C$, the phase flip should be performed on the spatial mode DOF of photon A. Thus the photon fusion can be deterministically completed.

Similar to the disentangling circuit shown in Figs. 2(b) and 3(b), all the quantum measurements M_{e_1}, M_{e_2}, M_B, and

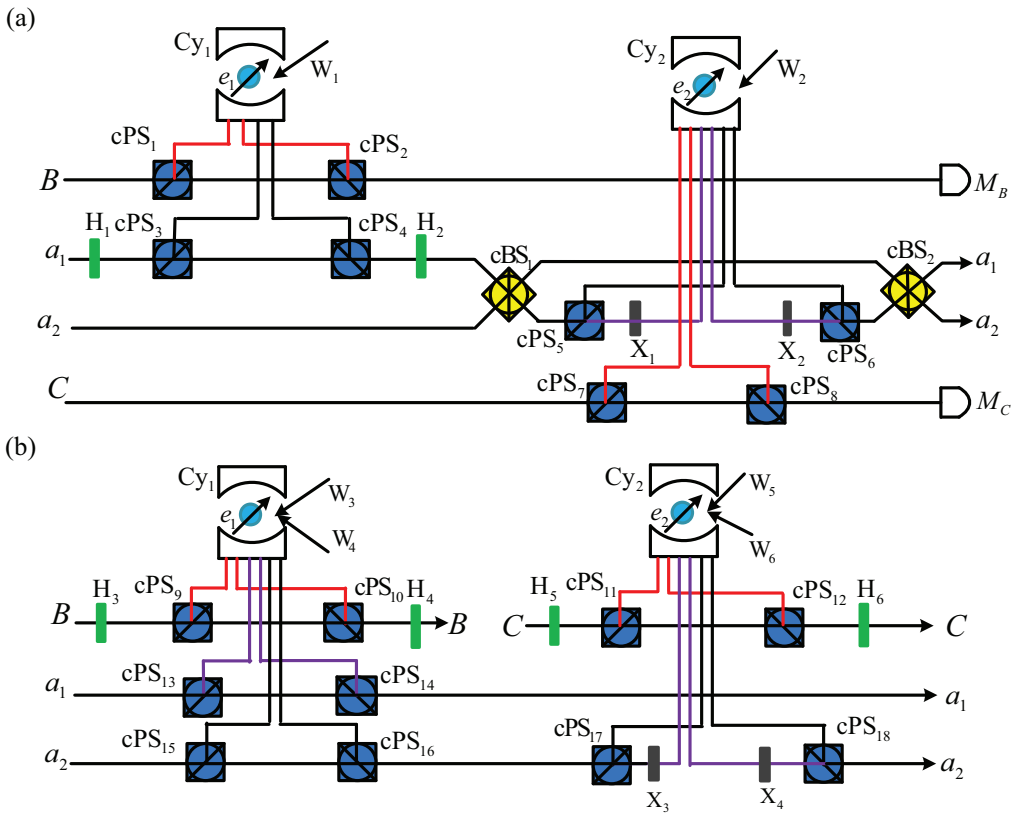

FIG. 4. (Color online) (a) Photon fusion based on the measurement feedback. a_i denote the spatial modes of an auxiliary photon A in the state $|R\rangle|a_1\rangle$. e_i denote the auxiliary quantum-dot spins in the state $|+\rangle$. cPS_i, H_i, X_i, cBS_i, and W_i are the same as those defined in Fig. 2. (b) Schematic disentangling circuit. If there are two input lines of one cavity, the photon represented with the red lines passes through the cavity first, and then the photon represented with the black lines passes through the cavity. If there are three input lines of one cavity, the photon represented with the red lines passes through the cavity first, and then the photon represented with the purple lines passes through the cavity while the photon represented with the black lines passes through the cavity last.

M_C may be avoided to get invertible quantum joining. The detailed disentangling circuit is shown in Fig. 4(b). For the entanglement shown in Eq. (21), the evolution procedure is defined as follows:

$$\begin{aligned}
&(\alpha|R\rangle_A|R\rangle_B|\uparrow\rangle_{e_1}+\beta|L\rangle_A|L\rangle_B|\downarrow\rangle_{e_1})\\
&\quad\otimes(\gamma|R\rangle_C|a_1\rangle|\uparrow\rangle_{e_2}+\delta|L\rangle_C|a_2\rangle|\downarrow\rangle_{e_2})\\
&\xrightarrow{H_3,\ldots,H_4}(\alpha|\uparrow\rangle_{e_1}|R\rangle_A+\beta|\downarrow\rangle_{e_1}|L\rangle_A)|R\rangle_B\\
&\quad\otimes(\gamma|\uparrow\rangle_{e_2}|R\rangle_C|a_1\rangle+\delta|\downarrow\rangle_{e_2}|L\rangle_C|a_2\rangle)\\
&\xrightarrow{H_5,\ldots,H_6}(\alpha|R\rangle_A|\uparrow\rangle_{e_1}+\beta|L\rangle_A|\downarrow\rangle_{e_1})|R\rangle_B\\
&\quad\otimes(\gamma|a_1\rangle|\uparrow\rangle_{e_2}+\delta|a_2\rangle|\downarrow\rangle_{e_2})|R\rangle_C\\
&\xrightarrow{W_3,\ldots,W_4}(\alpha|R\rangle_A+\beta|L\rangle_A)|R\rangle_B|\uparrow\rangle_{e_1}\\
&\quad\otimes(\gamma|a_1\rangle|\uparrow\rangle_{e_2}+\delta|a_2\rangle|\downarrow\rangle_{e_2})|R\rangle_C\\
&\xrightarrow{W_5,\ldots,W_6}(\alpha|R\rangle_A+\beta|L\rangle_A)(\gamma|a_1\rangle+\delta|a_2\rangle)\\
&\quad\otimes|R\rangle_B|R\rangle_C|\uparrow\rangle_{e_1}|\uparrow\rangle_{e_2}. \qquad (23)
\end{aligned}$$

Here, the subcircuit of photon B and the spin e_1 from the H_3 to H_4 is the same as the subcircuit of photon B and spin e' from H_3 to H_4 shown in Fig. 3(b), which has realized the CNOT gate shown in Eq. (17). The subcircuit of photon C and spin e_2 from H_5 to H_6 is the same as the subcircuit of photon B and spin e' from H_3 to H_4 shown in Fig. 2(b), which has realized the CNOT gate shown in Eq. (17). The subcircuit of photon A and spin e_1 from W_3 to W_4 is the same as the subcircuit of photon A and spin e_1 from W_1 to W_2 shown in Fig. 2(b), which has realized the CNOT gate shown in Eq. (18). The subcircuit of photon A and spin e_2 from W_5 to W_6 is the same as the subcircuit of photon A and spin e_2 from W_3 to W_4 shown in Fig. 2(b), which has realized the CNOT gate shown in Eq. (19). Therefore, by combining the circuits shown in Fig. 4, two circular-polarizing photons can be joined into one photon state with two DOFs without any measurement feedback. It means that the fusion is unitary.

VI. ELEMENTARY GATES REALIZED BY A PHOTON SYSTEM WITH TWO DOFS

With the present quantum fusion constructions, a two-qubit system of the quantum-dot spin and photon may be represented by one photon with two DOFs. The joined photon system may be very useful because of its superiority in quantum-information processing. Moreover, some quantum logic gates of two input qubits may be easily realized on the joined system. Typical examples are the CNOT gate and SWAP gate of a two-qubit system, and Toffoli gate of a three-qubit system, which are universal logic gates for quantum applications [22–33,40–43], shown in Fig. 5.

Consider an arbitrary photon $\alpha_1|R\rangle|a_1\rangle+\alpha_2|L\rangle|a_1\rangle+\alpha_3|R\rangle|a_2\rangle+\alpha_4|L\rangle|a_2\rangle$ with the polarization and spatial mode DOFs. One CNOT gate shown in Fig. 5(a) has realized the following transformation

$$|R\rangle\langle R|(|a_1\rangle\langle a_1|+|a_2\rangle\langle a_2|)+|L\rangle\langle L|(|a_2\rangle\langle a_1|+|a_1\rangle\langle a_2|) \qquad (24)$$

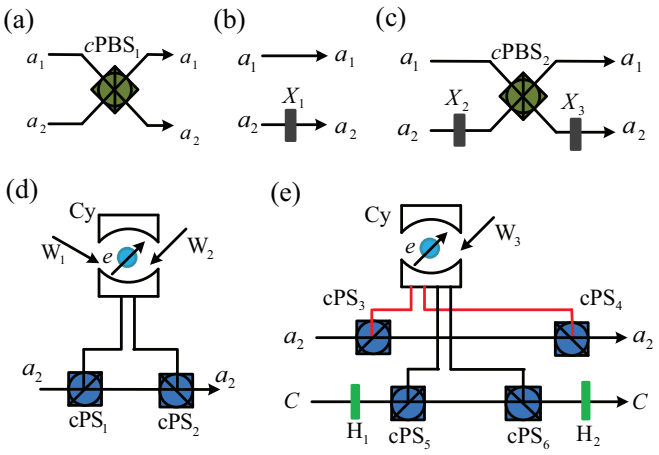

FIG. 5. (Color online) Elementary logic gates on one photon state with two DOFs. (a) CNOT gate. The polarization qubit is the controlling qubit while the spatial qubit is the target qubit. (b) CNOT gate. The polarization qubit is the target qubit while the spatial qubit is the controlling qubit. (c) SWAP gate. cPS_i, H_i, X_i, and W_i are the same as those defined in Fig. 2. (d) Toffoli gate. The photon with two DOFs is the controlling qubit while the electron spin is the target qubit. (e) Toffoli gate. The photon with two DOFs is controlling qubit while the photon with only a polarization DOF is the target qubit. cPBS_i represents the polarizing beam splitter in the circular basis, which transmits the photon in polarization $|L\rangle$ and reflects the photon in polarization $|R\rangle$, respectively.

using the circular-polarizing beam splitter cPBS_1. The other CNOT gate shown in Fig. 5(b) is defined by

$$|a_1\rangle\langle a_1|(|R\rangle\langle R|+|L\rangle\langle L|)+|a_2\rangle\langle a_2|(|R\rangle\langle L|+|L\rangle\langle R|) \qquad (25)$$

using the flip operation X_1 on the polarization DOF. The SWAP gate shown in Fig. 5(c) is defined by

$$\begin{aligned}
&\alpha_1|R\rangle|a_1\rangle+\alpha_2|L\rangle|a_1\rangle+\alpha_3|R\rangle|a_2\rangle+\alpha_4|L\rangle|a_2\rangle\\
&\xrightarrow[X_3]{X_2,\mathrm{cPBS}_2}\alpha_1|R\rangle|a_1\rangle+\alpha_2|R\rangle|a_2\rangle+\alpha_3|L\rangle|a_1\rangle+\alpha_4|L\rangle|a_2\rangle. \qquad (26)
\end{aligned}$$

The first Toffoli gate is performed on photon A and one quantum spin e in the state $|\psi\rangle=(\beta_1|\uparrow\rangle+\beta_2|\downarrow\rangle)$. Here, the target qubit is the quantum spin e, and the detailed circuit is shown in Fig. 5(d). The joint system of photon A and spin e changes as follows.

$$\begin{aligned}
|\phi\rangle_A|\psi\rangle_e&\xrightarrow{W_1}|\phi\rangle_A(\beta_1|+\rangle+\beta_2|-\rangle)_e\\
&\xrightarrow[\mathrm{cPS}_2]{\mathrm{cPS}_1,\mathrm{Cy}}\alpha_1|R\rangle|a_1\rangle(\beta_1|+\rangle+\beta_2|-\rangle)_e\\
&\quad+\alpha_2|L\rangle|a_1\rangle(\beta_1|+\rangle+\beta_2|-\rangle)_e\\
&\quad+\alpha_3|R\rangle|a_2\rangle(\beta_1|+\rangle+\beta_2|-\rangle)_e\\
&\quad+\alpha_4|L\rangle|a_2\rangle(\beta_1|-\rangle+\beta_2|+\rangle)_e\\
&\xrightarrow{W_2}(\alpha_1|R\rangle|a_1\rangle+\alpha_2|L\rangle|a_1\rangle)(\beta_1|\uparrow\rangle+\beta_2|\downarrow\rangle)_e\\
&\quad+\alpha_3|R\rangle|a_2\rangle(\beta_1|\uparrow\rangle+\beta_2|\downarrow\rangle)_e\\
&\quad+\alpha_4|L\rangle|a_2\rangle(\beta_1|\downarrow\rangle+\beta_2|\uparrow\rangle)_e, \qquad (27)
\end{aligned}$$

which is a Toffoli gate on two DOFs of photon A and spin e.

The second Toffoli gate is performed on photon A and a photon B in the state $|\phi\rangle_B = (\beta_1|R\rangle + \beta_2|L\rangle)$. Here, the target qubit is photon B, and the detailed circuit is shown in Fig. 5(e). The joint system of photon A and spin e changes as follows with the help of one spin with initial state $|+\rangle_e$.

$$
\begin{aligned}
&|\phi\rangle_A|\psi\rangle_B\ |+\rangle_e \\
&\xrightarrow[\text{cPS}_4]{\text{cPS}_3,\text{Cy}} [\alpha_1|R\rangle|a_1\rangle + \alpha_2|L\rangle|a_1\rangle + \alpha_3|R\rangle|a_2\rangle)|+\rangle_e \\
&\qquad + \alpha_4|L\rangle|a_2\rangle|-\rangle_e]|\phi\rangle_B \\
&\xrightarrow{W_3} [\alpha_1|R\rangle|a_1\rangle + \alpha_2|L\rangle|a_1\rangle + \alpha_3|R\rangle|a_2\rangle)|\uparrow\rangle_e \\
&\qquad + \alpha_4|L\rangle|a_2\rangle|\downarrow\rangle_e]|\phi\rangle_B \\
&\xrightarrow{H_1} [(\alpha_1|R\rangle|a_1\rangle + \alpha_2|L\rangle|a_1\rangle + \alpha_3|R\rangle|a_2\rangle)|\uparrow\rangle_e \\
&\qquad + \alpha_4|L\rangle|a_2\rangle|\downarrow\rangle_e](\beta_1'|R\rangle + \beta_2'|L\rangle)_B \\
&\xrightarrow[\text{cPS}_6]{\text{cPS}_5,\text{Cy}} \beta_1'|R\rangle_B(\alpha_1|R\rangle|a_1\rangle|\uparrow\rangle_e + \alpha_2|L\rangle|a_1\rangle|\uparrow\rangle_e \\
&\qquad + \alpha_3|R\rangle|a_2\rangle|\uparrow\rangle_e + \alpha_4|L\rangle|a_2\rangle|\downarrow\rangle_e) \\
&\qquad + \beta_2'|L\rangle_B(\alpha_1|R\rangle|a_1\rangle|\uparrow\rangle_e + \alpha_2|L\rangle|a_1\rangle|\uparrow\rangle_e \\
&\qquad + \alpha_3|R\rangle|a_2\rangle|\uparrow\rangle_e - \alpha_4|L\rangle|a_2\rangle|\downarrow\rangle_e) \\
&\xrightarrow{H_2} (\alpha_1|R\rangle|a_1\rangle + \alpha_2|L\rangle|a_1\rangle + \alpha_3|R\rangle|a_2\rangle) \\
&\qquad \otimes|\uparrow\rangle_e(\beta_1|R\rangle + \beta_2|L\rangle)_B \\
&\qquad + \alpha_4|L\rangle|a_2\rangle|\downarrow\rangle_e(\beta_1|L\rangle + \beta_2|R\rangle)_B, \qquad (28)
\end{aligned}
$$

which may collapse into

$$
\begin{aligned}
&(\alpha_1|R\rangle|a_1\rangle + \alpha_2|L\rangle|a_1\rangle + \alpha_3|R\rangle|a_2\rangle)(\beta_1|R\rangle + \beta_2|L\rangle)_B \\
&\quad + \alpha_4|L\rangle|a_2\rangle(\beta_1|L\rangle + \beta_2|R\rangle)_B \qquad (29)
\end{aligned}
$$

using the spin measurement M_e under the basis $\{|\pm\rangle\}$. Here, $\beta_1' = (\beta_1 + \beta_2)/\sqrt{2}$, $\beta_2' = (\beta_1 - \beta_2)/\sqrt{2}$, and the phase flip $|R\rangle\langle R| - |L\rangle\langle L|$ is performed on photon A from the spatial mode a_2 for the measurement outcome $|-\rangle_e$. It has completed the Toffoli gate on two DOFs of photon A and photon B. Furthermore, all the present quantum fusion schemes can be realized unitarily, which means that joining procedures are invertible. Thus one photon with two DOFs may be easily split into the joint system of the quantum-dot spin and photon by inverting our circuits shown in Figs. 2–4. These simple implementations may be explored up to specific applications.

VII. DISCUSSION AND CONCLUSION

Under the ideal condition, the cavity side leakage may be neglected, i.e., $|r_0| \approx 1$ and $|r| \approx 1$. All the fidelities of the present joining schemes are 100%. However, the side leakage from the cavity cannot be neglected in experiment [45,46,49–64]. Under the resonant condition, the optical selection rule of the cavity system shown in Eq. (5) may become

$$
\begin{aligned}
&|R\rangle|\uparrow\rangle \mapsto |r_0||R\rangle|\uparrow\rangle, |R\rangle|\downarrow\rangle \mapsto |r||R\rangle|\downarrow\rangle, \\
&|L\rangle|\uparrow\rangle \mapsto |r||L\rangle|\uparrow\rangle, |L\rangle|\downarrow\rangle \mapsto |r_0||L\rangle|\downarrow\rangle \qquad (30)
\end{aligned}
$$

in experiment. From this new rule, the joining fidelity is reduced to $F = |\langle\Psi_f|\Psi_i\rangle|^2$, where $|\Psi_i\rangle$ is the ideal output photon system while $|\Psi_f\rangle$ is the output photon system from our fused schemes. The fidelities of our joining schemes are evaluated

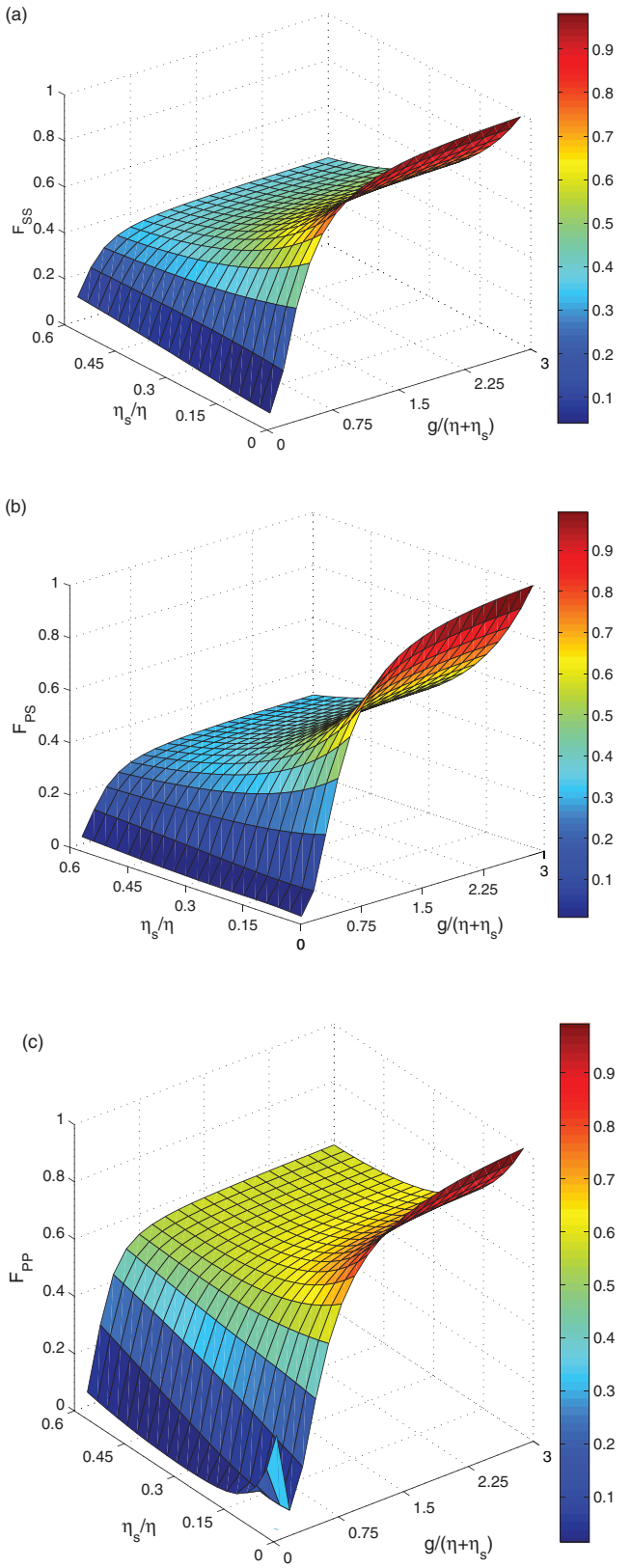

FIG. 6. (Color online) (a) The average fidelity F_{SS} of spin joining versus η_s/η and $g/(\eta+\eta_s)$. (b) The average fidelity F_{PS} of photon-spin joining versus η_s/η and $g/(\eta+\eta_s)$. (c) The average fidelity F_{PP} of photon joining versus η_s/η and $g/(\eta+\eta_s)$. The coupling strength is defined by $\varsigma = 0.1\eta_s$.

and shown in Fig. 6. Moreover, by defining the efficiency P as the detecting probability of the photons after the joining schemes, the efficiencies are also evaluated and shown in Fig. 7. One can see that the cavity side leakage has a great impact on the fidelities and efficiencies. When $\eta_s \ll \eta$, these joining schemes work efficiently even in a weak coupling regime. When $\eta_s \ll \eta$ is satisfied, efficient joining schemes work only in a strong coupling regime defined by $g > (\eta + \eta_s)/4$. It is challenging to achieve a strong coupling experimentally. Fortunately, $g/(\eta + \eta_s)$ has been raised to 2.4 by engineering the sample designs, growth, and fabrication in 1.5 μm micropillar microcavities [55]. For these joining schemes, all the fidelities are greater than 95% and all the efficiencies are greater than 67% when $\eta_s/\eta \approx 0.25$ and $g/(\eta + \eta_s) \approx 2.4$. Both the fidelity and the efficiency become high when η_s/η becomes smaller. High-efficiency joining schemes may be also achieved with a small η_s/η in a strong coupling regime.

Experimental fidelity and efficiency may be slightly decreased because of spin decoherence and trion dephasing [49,50]. However, when the hole spin coherence time is longer than three orders of the cavity photon lifetime [58], the hole spin dephasing may be neglected. The Hadamard transformation of the spin in these joining schemes can be realized by using a nanosecond spin resonance microwave pulse [56] and spin echo technique [60] to protect the spin coherence. Moreover, by engineering the shape, size, and type of charged exciton [60], the heavy-light hole mixing may be reduced. Furthermore, optical dephasing has a negligible impact on these joining schemes when the optical coherence time of an exciton is longer than ten times the cavity photon lifetime x. The optical selection rule has been experimentally realized with the spin state of a single trapped atom and the polarization state [63]. Based on this rule, they have constructed the controlled phase flip and CNOT on the joint system of the atom state and the polarization state [64]. Their gates may be explored to implement our schemes. Of course, the present joining schemes are also conditional on the flawless features of several elements and setups in the experiment, which include the perfect overlap of the cavity mode with the two spatially separated optical beams, the phase stability of the interferometer composed of the cBS, and the perfect time overlap of two beams passing through several interferometers.

In conclusion, we have investigated the quantum joining and quantum splitting schemes introduced by Vitelli *et al.* in Refs. [29,33]. The deterministic quantum-dot spin joining, photon and quantum-dot spin joining, and photon joining may be completed by using the optical selection rule induced by the one-sided optical microcavity. By adjusting the frequencies of the input photon and cavity mode, a phase difference $\theta_0 - \theta_f \approx \pi$ may be achieved. Moreover, in order to obtain an ideal optical selection transformation, the side leakage and cavity loss rate η_s/η should be controlled to be as small as possible. Thus the input quantum information of quantum-dot spins or photons may be represented by a new photon with two DOFs in the feed-forward mechanism. These schemes are easily extended to invertible quantum splitting schemes by replacing the quantum-dot measurement or the photon measurement with the corresponding disentangling

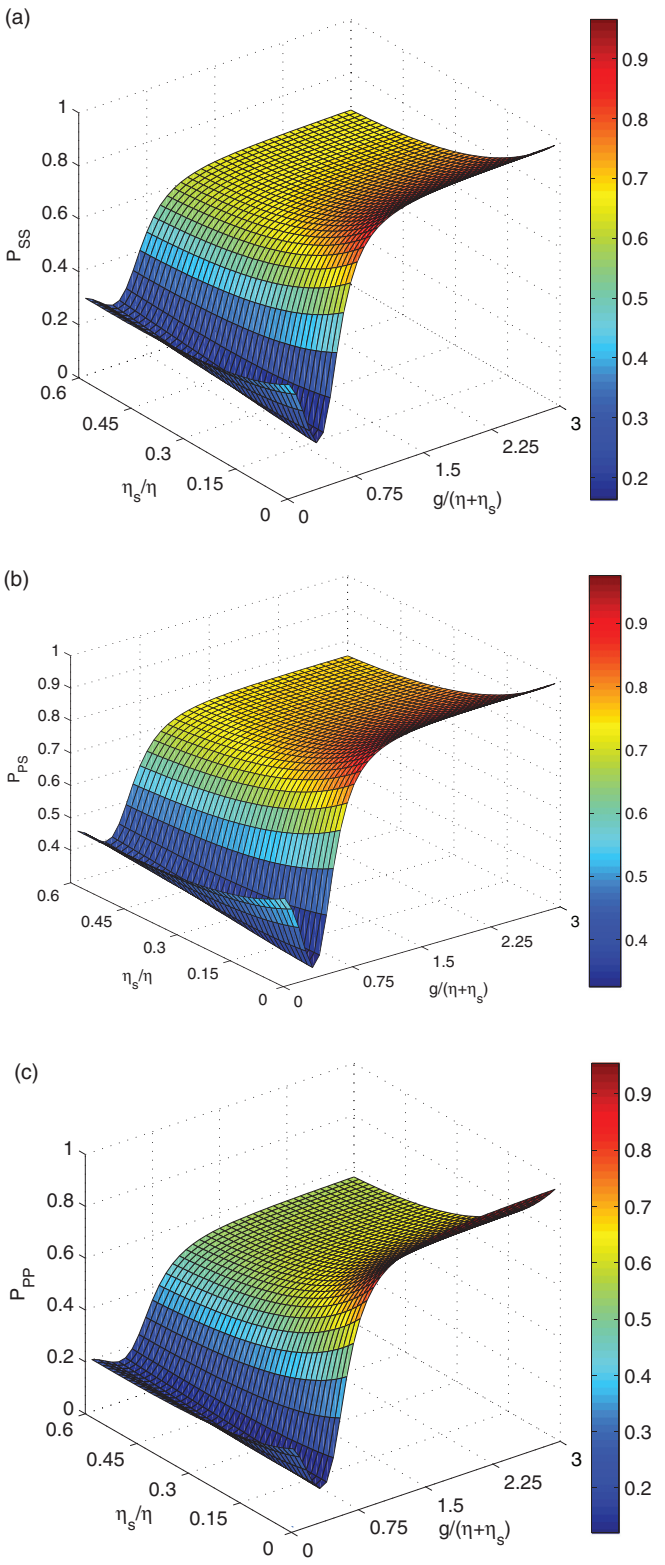

FIG. 7. (Color online) (a) The efficiency P_{SS} of spin joining versus η_s/η and $g/(\eta + \eta_s)$. (b) The efficiency P_{PS} of photon-spin joining versus η_s/η and $g/(\eta + \eta_s)$. (c) The efficiency P_{PP} of photon joining versus η_s/η and $g/(\eta + \eta_s)$. The coupling strength is defined by $\varsigma = 0.1\eta_s$.

circuit. From previous experiments [49,50,53–64], the present schemes are feasible in experiment with current technology. Compared with the photonic joining scheme [29,33], our modified schemes are more flexible for quantum computation and quantum network communication because of different superiorities of the quantum-dot spin and photon.

ACKNOWLEDGMENTS

This work is supported by the National Natural Science Foundation of China (No. 61303039, No. 61272514, No. 61201253, No. 61121061, No. 61161140320), NCET (No. NCET-13-0681), the Fok Ying Tong Education Foundation (No. 131067), Open Foundation of State key Laboratory of Networking and Switching Technology (Beijing University of Posts and Telecommunications) (No. SKLNST-2013-1-11), the National Development Foundation for Cryptological Research (No. MMJJ201401012), Fundamental Research Funds for the Central Universities (No. 2682014CX095), and Science Foundation Ireland (SFI) under the International Strategic Cooperation Award Grant No. SFI/13/ISCA/2845.

[1] P. W. Shor, SIAM J. Comput. **26**, 1484 (1997).
[2] L. K. Grover, Phys. Rev. Lett. **79**, 325 (1997).
[3] E. Farhi, J. Goldstone, S. Gutmann, J. Lapan, A. Lundgren, and D. Preda, Science **292**, 472 (2001).
[4] S. Lloyd, M. Mohseni, and P. Rebentrost, Nat. Phys. **10**, 631 (2014).
[5] C. H. Bennett and G. Brassard, in *Proceedings of the IEEE International Conference Computers, Systems and Signal Processing, Bangalore, India* (IEEE, New York, 1984), p. 175.
[6] M. Hillery, V. Buzek, and A. Berthiaume, Phys. Rev. A **59**, 1829 (1999).
[7] C. H. Bennett and D. P. DiVincenzo, Nature **404**, 247 (2000).
[8] T. Tyc and B. C. Sanders, Phys. Rev. A **65**, 042310 (2002).
[9] A. V. Sergienko, *Quantum Communications and Cryptography* (Taylor & Francis, London, 2006).
[10] T. D. Ladd, F. Jelezko, R. Laamme, Y. Nakamura, C. Monroe, and J. L. O'Brien, Nature **464**, 45 (2010).
[11] P. Kok, W. J. Munro, K. Nemoto, T. C. Ralph, J. P. Dowling, and G. J. Milburn, Rev. Mod. Phys. **79**, 135 (2007).
[12] J. L. O'Brien, A. Furusawa, and J. Vuckovic, Nat. Photon. **3**, 687 (2009).
[13] J.-W. Pan, Z.-B. Chen, C.-Y. Lu, H. Weinfurter, A. Zeilinger, and M. Zukowski, Rev. Mod. Phys. **84**, 777 (2012).
[14] M. Müler, S. Bounouar, K. D. Jös, M. Gläsl, and P. Michler, Nat. Photon. **8**, 224 (2014).
[15] Y.-F. Huang, B.-H. Liu, L. Peng, Y.-H. Li, L. Li, C.-F. Li, and G.-C. Guo, Nat. Commun. **2**, 546 (2011).
[16] X.-C. Yao, T.-X. Wang, P. Xu, H. Lu, G.-S. Pan, X.-H. Bao, C.-Z. Peng, C.-Y. Lu, Y.-A. Chen, and J.-W. Pan, Nat. Photon. **6**, 225 (2012).
[17] J. T. Barreiro, J.-D. Bancal, P. Schindler, D. Nigg, M. Hennrich, T. Monz, N. Gisin, and R. Blatt, Nat. Phys. **9**, 559 (2013).
[18] A. Mair, V. Alipasha, G. Weihs, and A. Zeilinger, Nature **412**, 313 (2001).
[19] D. Bruss and C. Macchiavello, Phys. Rev. Lett. **88**, 127901 (2002).
[20] P. Hariharan and B. C. Sanders, Optics Express **10**, 1222 (2002).
[21] M. Fujiwara, M. Takeoka, J. Mizuno, and M. Sasaki, Phys. Rev. Lett. **90**, 167906 (2003).
[22] B. P. Lanyon, M. Barbieri, M. P. Almeida, T. Jennewein, T. C. Ralph, K. J. Resch, G. J. Pryde, J. L. O'Brien, A. Gilchrist, and A. G. White, Nat. Phys. **5**, 134 (2009).
[23] R. Ceccarelli, G. Vallone, F. De Martini, P. Mataloni, and A. Cabello, Phys. Rev. Lett. **103**, 160401 (2009).
[24] S. Straupe and S. Kulik, Nat. Photon. **4**, 585 (2010).
[25] C. Bonato, F. Haupt, S. S. R. Oemrawsingh, J. Gudat, D. Ding, M. P. van Exter, and D. Bouwmeester, Phys. Rev. Lett. **104**, 160503 (2010).
[26] M.-X. Luo and X. Wang, Sci. Rep. **4**, 5732 (2014).
[27] W.-B. Gao, C.-Y. Lu, X.-C. Yao, P. Xu, O. Guhne, A. Goebel, Y.-A. Chen, C.-Z. Peng, Z.-B. Chen, and J.-W. Pan, Nat. Phys. **6**, 331 (2010).
[28] A. C. Dada, J. Leach, G. S. Buller, M. J. Padgett, and E. Andersson, Nat. Phys. **7**, 677 (2011).
[29] C. Vitelli, N. Spagnolo, L. Aparo, F. Sciarrino, E. Santamato, and L. Marrucci, Nat. Photon. **7**, 521 (2013).
[30] E. Knill, R. Laamme, and G. J. Milburn, Nature **409**, 46 (2001).
[31] T. B. Pittman, M. J. Fitch, B. C. Jacobs, and J. D. Franson, Phys. Rev. A **68**, 032316 (2003).
[32] S. Gasparoni, J.-W. Pan, P. Walther, T. Rudolph, and A. Zeilinger, Phys. Rev. Lett. **93**, 020504 (2004).
[33] E. Passaro, C. Vitelli, N. Spagnolo, F. Sciarrino, E. Santamato, and L. Marrucci, Phys. Rev. A **88**, 062321 (2013).
[34] J. C. García-Escartín and P. Chamorro-Posada, Phys. Rev. A **78**, 062320 (2008).
[35] M. Grace, C. Brif, H. Rabitz, I. Walmsley, R. Kosut, and D. Lidar, New J. Phys. **8**, 35 (2006).
[36] B. Julsgaard, J. Sherson, J. I. Cirac, J. Fiurasek, and E. S. Polzik, Nature **432**, 482 (2004).
[37] T. Chanelière, D. N. Matsukevich, S. D. Jenkins, S.-Y. Lan, T. A. B. Kennedy, and A. Kuzmich, Nature **438**, 833 (2005).
[38] H. J. Kimble, Nature **453**, 1023 (2008).
[39] S. Ritter, C. Nöleke, C. Hahn, A. Reiserer, A. Neuzner, M. Uphoff, M. Müke, E. Figueroa, J. Bochmann, and G. Rempe, Nature **484**, 195 (2012).
[40] J. Q. You, J. S. Tsai, and F. Nori, Phys. Rev. Lett. **89**, 197902 (2002).
[41] J. H. Plantenberg, P. C. de Groot, C. J. P. M. Harmans, and J. E. Mooij, Nature **447**, 836 (2007).
[42] M. Marjanska, I. L. Chuang, and M. G. Kubinec, J. Chem. Phys. **112**, 5095 (2000).
[43] F. Schmidt-Kaler, H. Häfner, M. Riebe, S. Gulde, G. P. T. Lancaster, T. Deuschle, C. Becher, C. F. Roos, J. Eschner, and R. Blatt, Nature **422**, 408 (2003).
[44] A. Auffèves-Garnier, C. Simon, J. M. Gérard, and J. P. Poizat, Phys. Rev. A **75**, 053823 (2007).
[45] J. I. Cirac, P. Zoller, H. J. Kimble, and H. Mabuchi, Phys. Rev. Lett. **78**, 3221 (1997).

[46] E. Waks and J. Vuckovic, Phys. Rev. Lett. **96**, 153601 (2006).
[47] G. Chen, C. F. Li, Z. Q. Yin, Y. Zou, L. X. He, and G. C. Guo, Europhys. Lett. **89**, 44002 (2010).
[48] T. J. Wang, Y. Zhang, and C. Wang, Laser Phys. Lett. **11**, 025203 (2014).
[49] C. Y. Hu, W. J. Munro, and J. G. Rarity, Phys. Rev. B **78**, 125318 (2008).
[50] C. Y. Hu, W. J. Munro, J. L. O'Brien, and J. G. Rarity, Phys. Rev. B **80**, 205326 (2009).
[51] T. J. Wang, Y. Lu, and G. L. Long, Phys. Rev. A **86**, 042337 (2012).
[52] T. Wang and C. Wang, J. Opt. Soc. Am. B **30**, 2689 (2013).
[53] L.-M. Duan and H. J. Kimble, Phys. Rev. Lett. **92**, 127902 (2004).
[54] J. P. Reithmaier, G. Søo, A. Löfler, C. Hofmann, S. Kuhn, S. Reitzenstein, L. V. Keldysh, V. D. Kulakovskii, T. L. Reinecke, and A. Forchel, Nature **432**, 197 (2004).
[55] T. Yoshie, A. Scherer, J. Hendrickson, G. Khitrova, H. M. Gibbs, G. Rupper, C. Ell, O. B. Shchekin, and D. G. Deppe, Nature **432**, 200 (2004).
[56] J. R. Petta, A. C. Johnson, J. M. Taylor, E. A. Laird, A. Yacoby, M. D. Lukin, C. M. Marcus, M. P. Hanson, and A. C. Gossard, Science **309**, 2180 (2005).
[57] C. Y. Hu, A. Young, J. L. O'Brien, W. J. Munro, and J. G. Rarity, Phys. Rev. B **78**, 085307 (2008).
[58] D. Brunner, B. D. Gerardot, P. A. Dalgarno, G. Wüst, K. Karrai, N. G. Stoltz, P. M. Petroff, and R. J. Warburton, Science **325**, 70 (2009).
[59] A. B. Young, R. Oulton, C. Y. Hu, A. C. T. Thijssen, C. Schneider, S. Reitzenstein, M. Kamp, S. Höfling, L. Worschech, A. Forchel, and J. G. Rarity, Phys. Rev. A **84**, 011803 (2011).
[60] C. Y. Hu and J. G. Rarity, Phys. Rev. B **83**, 115303 (2011).
[61] W. Langbein, P. Borri, U. Woggon, V. Stavarache, D. Reuter, and A. D. Wieck, Phys. Rev. B **70**, 033301 (2004).
[62] D. F. Walls and G. J. Milburn, *Quantum Optics* (Springer-Verlag, Berlin, 2008).
[63] A. Reiserer, S. Ritter, and G. Rempe, Science **342**, 1349 (2013).
[64] A. Reiserer, N. Kalb, G. Rempe, and S. Ritter, Nature **508**, 237 (2014).